Synthesis, characterization and thermal decomposition study of some nickel nitro derivatives

A. Bolibar,[a] M. Insausti,[a] L. Lorente,[a] J. L. Pizarro,[b] M. I. Arriortua[b] and T. Rojo*[a]

[a]Departamento de Química Inorgánica, and [b]Departamento de Mineralogía-Petrología, Universidad del País Vasco, Apartado 644, 48080 Bilbao, Spain

Compounds with general formula $[K_xM_yNi(NO_2)_6(H_2O)_n]$ (M = Ca, Sr, Ba, La; $x = 0$–2; $y = 1$, 2; $n = 0$, 4) have been prepared and characterized by XRD, IR and EPR techniques. The structure of $[Ba_2Ni(NO_2)_6(H_2O)_2]\cdot 2H_2O$ has been determined by single crystal X-ray diffraction: space group $P6_3$, $a = 7.525(1)$ Å and $c = 14.516(1)$ Å. The geometry of the compound consists of an intricate network of ligand-bridged coordination polyhedra, where the arrangement of the nickel(II) ion exhibits a slightly distorted octahedral topology. The Ca, Sr and La phases have been indexed with a cubic cell, space group $Pm3\,m$ and cell parameters 10.354(5) Å, 10.517(5) Å and 10.571(8) Å, respectively. Thermal decomposition of the different compounds using TG involves two consecutive steps: ligand pyrolysis and evolution of the inorganic residue. For the barium compound a third step appears which corresponds to the dehydration process. Further thermal treatments in tubular furnaces yield the formation of different mixed oxides of Ni^{III} and Ni^{IV} at lower pressures of oxygen than those obtained from the ceramic method. Advantages of using the metallo–organic method can also be deduced from the SEM study.

Introduction

In the last few years the $RNiO_3$ (R = rare-earth metal) phases have attracted considerable attention since they are among the few transition metal oxides that exhibit metallic properties or metal-to-insulator (MI) transitions.[1] The transition temperature T_{MI} systematically rises when the rare-earth-metal size becomes smaller, as the distortion of the perovskite with respect to the ideal structure increases.[2] In this way, $LaNiO_3$, which shows a slightly distorted rhombohedral structure, keeps its metallic character down to 1.5 K, showing no MI transition.[3] Related to these compounds, other nickel oxides have long being investigated because of their low dimensionality. Among these, the M–Ni–O phases, where M is an alkaline-earth metal,[4–6] must be mentioned.

These oxides have been traditionally prepared by the ceramic method and, in some cases, high pressures of oxygen have been employed with the aim of obtaining trivalent and tetravalent nickel oxides. Nevertheless, in the past alternative strategies have been used to improve the final mixed oxides. Among these, the use of metallo–organic precursors could be considered as one of the best alternative methods because they allow the synthesis of different oxides at the molecular level, with diffusion distances in the range 2–20 Å.[7] As a result, the phases can be obtained using shorter heating times and lower temperatures than those used for the conventional ceramic method. Moreover, suitable precursors would result in significant modifications in the microstructure of the final products.[8,9]

To date, carboxylates have long been known and studied as binding agents; however, they have the disadvantage of incorporating very large amounts of carbon, which later must be removed.[10] In order to prepare suitable precursors for the nickel oxides we have chosen the nitrite ion as a ligand. This is a versatile ligand which forms a range of compounds of the $A_2B[Ni(NO_2)_6]$ form, where A is a monovalent cation, such as K^+, and B a divalent one.[11,12]

This paper reports the usefulness of the metallo–organic method for the soft synthesis of nickel oxides. For this purpose, different complexes with formulae $[Ba_2Ni(NO_2)_6(H_2O)_2]\cdot 2H_2O$, $[K_2SrNi(NO_2)_6]$, $[KLaNi(NO_2)_6]$ and $[K_2CaNi(NO_2)_6]$ have been synthesized and characterized. The decomposition of the compounds has been studied by TG. Taking these results into account, the complexes were heated at different temperatures to obtain the respective oxides. Scanning electron microscopy was performed to study the morphology of these phases.

Experimental

Synthesis of the compounds

$NaNO_2$ (40 mmol) was added to a solution of $Ni(NO_3)_2\cdot 6H_2O$ (5 mmol) and the mixture was stirred for 1 h, after which an aqueous solution of MCl_2 (M = Ca, Sr, Ba) or $LaCl_3$ was added. After several hours, crystalline powder compounds were obtained, filtered off and dried over P_2O_5 for 24 h. For the barium compound, crystals suitable for X-ray structure determination were obtained.

Physical measurements

Elemental analyses were performed using a Perkin-Elmer 240B microanalyzer. IR spectra were obtained with KBr pellets and Nujol mulls in the 400–4000 cm^{-1} range, using a MATTSON FTIR 1000 spectrophotometer. EPR spectra were recorded on a Bruker ESP 300 spectrometer, equipped with a standard Oxford low-temperature device operating at X and Q band frequencies. The magnetic field was measured with a Bruker BNM 200 gaussmeter, and the frequency was determined with an HP5352B microwave frequency counter. TG measurements were carried out with a Perkin-Elmer System-7 DSC–TG unit. Crucibles containing 20 mg of sample were heated at 10 °C min^{-1} under dry air and nitrogen. The powder X-ray diffraction (XRD) pattern was taken using a Stoe diffractometer equipped with a germanium monochromater (Cu-Kα_1 radiation). Data were collected by scanning in the range $10° < 2\theta < 90°$ with increments of 0.02° (2θ). Scanning electron microscopic (SEM) observations were also carried out to give some indication of the compactness of the oxide using a JEOL JSM-6400 instrument.

Crystal structure determination†

A hexagonal pale yellow crystal having approximate dimensions of $0.1 \times 0.7 \times 0.7$ mm was mounted on a glass fibre and

† Full atomic coordinates, bond lengths and angles, and thermal parameters have been deposited at the Cambridge Crystallographic Data Centre (CCDC). CCDC reference number 1145/49.

Table 1 Data collection and structure refinement of $[Ba_2Ni(NO_2)_6(H_2O)_2]\cdot 2H_2O$

formula	$H_8Ba_2N_6NiO_{16}$
crystal system	hexagonal
space group	$P6_3$
a/Å	7.5250(10)
c/Å	14.5160(10)
Z	2
M	681.54
V/Å^3	711.85(14)
D_m/g cm^{-3}	3.15(2)
D_{calc}/g cm^{-3}	3.18
μ(Mo-Kα)/mm^{-1}	6.887
$F(000)$	636
measurements	
λ(Mo-Kα)	0.71069
θ range°	2.81–29.91
no. measured reflections	4533
interval h, k, l	10, ±10, ±20
refinements	
no. variables	76
selection criterion	$I \geqslant 2.5\sigma(I)$
R(int)	1394
observed reflections	1344
weighting scheme	
$w=1/[\sigma^2(F_o^2)]$	
$R=(\Sigma\|\|F_o\|-\|F_c\|\|)/(\Sigma\|F_o\|)$	0.0536
$wR2=[\Sigma[w(F_o^2-F_c^2)^2]/\Sigma[w(F_o^2)^2]]^{1/2}$	0.0659

transferred to an Enraf-Nonius CAD-4 diffractometer with graphite-monochromated Mo-Kα radiation. The orientation matrix and the final lattice parameters were determined from 25 machine-centred high-angle reflections ($14° < 2\theta < 24°$). Crystallographic data and processing parameters are summarized in Table 1. Two standard reflections were recorded every 1 h. Their intensities showed no statistically significant change over the duration of the data collection. Lorentz and polarization corrections were applied. The structure was solved by direct methods using the program SHELXS86[13] and Fourier synthesis, isotropic least-squares refinement, using SHELXL93.[14] Further anisotropic refinements followed by a difference Fourier synthesis did not allow the location of all of the H atoms. Non-hydrogen atomic scattering factors were taken from *International Tables for X-ray Crystallography*.[15] The final difference Fourier map showed no peaks higher than 2.35 or deeper than −1.66 e Å^{-3}. The geometric calculations were performed with PARST[16] and molecular illustrations were drawn with ATOMS[17] and BALL&STICK.[18]

Results and Discussion

Description of the structure

The structure of the $[Ba_2Ni(NO_2)_6(H_2O)_2]\cdot 2H_2O$ compound may be described as a complex three-dimensional network of barium and nickel(II) ions, coordinated by nitro ligand bridges. In the unit cell, two non-equivalent water molecules are present. One of them, Ow(5), is coordinated to the barium atom and the other one, Ow(6), remains as crystallization water. A perspective drawing of the compound is shown in Fig. 1. Atomic coordinates and some selected bond distances and angles are given in Tables 2 and 3.

The nickel atom is octahedrally coordinated to six equivalent nitro groups, through the nitrogen atom (Fig. 2). In the equatorial positions, the N(1), N(1)[15], N(2)[16] and N(2)[15] atoms are present, the nickel(II) ion displacement from the mean plane being 0.005 Å. There are two different distances in the compound from the nickel atom; the N(1), N(1)[15] and N(1)[16] atoms are at 2.14(2) Å and the N(2), N(2)[15] and N(2)[16] atoms are at 2.06(2) Å. The distortion around the nickel(II) ion has been calculated by quantification of the Muetterties and Guggenberger description.[19] The value obtained, $\Delta = 0.03$, is indicative of a highly regular octahedron.

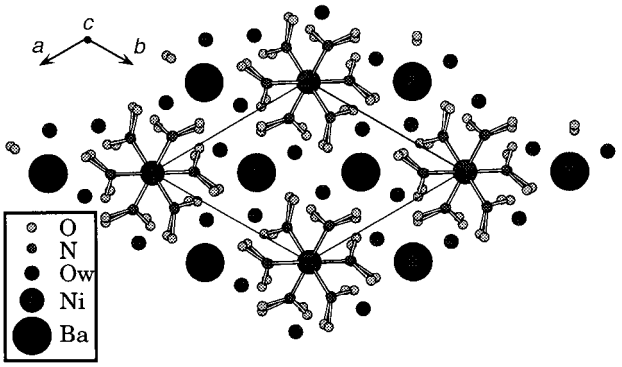

Fig. 1 A perspective view of the $[Ba_2Ni(NO_2)_6(H_2O)_2]\cdot 2H_2O$ compound in the *ab* plane

Table 2 Atomic coordinates and equivalent isotropic temperature factors (Å^2) for $[Ba_2Ni(NO_2)_6(H_2O)_2]\cdot 2H_2O$

atom	x	y	z	B_{eq}/Å^2
Ba(1)	0.6667	0.3333	0.2923(1)	16(1)
Ba(2)	0.6667	0.3333	0.6426(2)	20(1)
Ni	0.0000	0.0000	−0.1086(3)	12(1)
O(1)	−0.425(2)	−0.122(3)	−0.0441(2)	47(6)
O(2)	−0.272(3)	−0.232(6)	0.0457(1)	43(6)
O(3)	−0.015(3)	−0.302(3)	−0.251(1)	29(4)
O(4)	−0.301(4)	−0.395(3)	−0.187(3)	67(10)
O(5)	0.434(3)	0.344(3)	0.133(2)	30(4)
O(6)	0.6667	0.3333	−0.027(3)	5(4)
N(1)	−0.270(2)	−0.140(2)	−0.025(1)	12(3)
N(2)	−0.122(2)	−0.258(2)	−0.1901(9)	4(3)

$B_{eq} = 8/3\pi^2[U_{33} + 4/3(U_{11} + U_{22} - U_{12})]$.

In the ligands, the average N—O distances are 1.2 Å, except for N(2)—O(3) which is 1.34(2) Å. The average N—O—N angle is 117°. The *trans* ligands are coplanar and exhibit an arrangement similar to that observed for the $K_2A[Ni(NO_2)_6]$ salts, where A is Ba, Sr or Pb.[11] The Ni—N bond lengths and internal dimensions of the nitro groups are also very similar to those observed in other nickel(II) hexanitro complexes.[11]

The nitro ligands are bonded to different barium ions by the oxygen atoms, so that they serve as bridges to hold the tridimensional network. In all cases, two barium atoms are linked to each oxygen, except for the O(2) atom which is coordinated to Ba(2).[17] In this way, twelve oxygen atoms form the coordination polyhedron of the barium ions with maximum and minimum distances of 3.03(2) Å and 2.82(2) Å for the O(4) and O(3) atoms, respectively. Some of these oxygen atoms are from water molecules, Ow(5), and they are also bonded to other barium atoms forming the tridimensional network.

In the case of the Ca, Sr and La phases, high quality crystals were not obtained. X-Ray diffraction patterns of the microcrystalline products were performed and indexation was made by FULLPROF (pattern matching analysis)[20] in the range $2\theta =$ 10–90°. The spectra were indexed on the basis of a cubic cell, space group $Pm3\,m$ with cell parameters of 10.517(5) Å, 10.354(5) Å and 10.571(8) Å for $[K_2SrNi(NO_2)_6]$, $[K_2CaNi(NO_2)_6]$ and $[KLaNi(NO_2)_6]$, respectively.

IR and EPR spectroscopies

The interest of the IR spectra lies in the bands of the NO_2^- group. In the nitro species, the bands corresponding to the ν_s symmetric and ν_{as} antisymmetric vibrations appear in the 1320–1340 cm^{-1} and 1370–1470 cm^{-1} ranges, respectively. However, in the nitrite species, the two bands appear at

Table 3 Some selected bond distances (Å) and angles (°) with e.s.d.s in parentheses for $[Ba_2Ni(NO_2)_6(H_2O)_2]\cdot 2H_2O$

Ni—N(2)	2.06(2)	N(1)—O(1)	1.27(2)
Ni—N(2)^{15}	2.06(2)	N(1)—O(2)	1.23(3)
Ni—N(2)^{16}	2.06(2)	N(2)—O(3)	1.34(2)
Ni—N(1)^{15}	2.14(2)	N(2)—O(4)	1.22(3)
Ni—N(1)^{16}	2.14(2)		
Ni—N(1)	2.14(2)		
Ba(1)—O(3)^{1}	2.82(2)	Ba(2)—O(4)^{13}	3.13(3)
Ba(1)—O(3)^{2}	2.82(2)	Ba(2)—O(5)^{9}	2.88(2)
Ba(1)—O(3)^{3}	2.82(2)	Ba(2)—O(5)^{10}	2.88(2)
Ba(1)—Ow(5)^{4}	2.92(2)	Ba(2)—O(5)^{11}	2.88(2)
Ba(1)—Ow(5)^{5}	2.92(2)	Ba(2)—O(3)^{12}	3.02(2)
Ba(1)—Ow(5)	2.92(2)	Ba(2)—O(3)^{13}	3.02(2)
Ba(1)—O(1)^{6}	2.93(2)	Ba(2)—O(3)^{14}	3.02(2)
Ba(1)—O(1)^{7}	2.93(2)	Ba(2)—O(2)^{6}	3.02(2)
Ba(1)—O(1)^{8}	2.93(2)	Ba(2)—O(2)^{8}	3.02(2)
Ba(1)—O(4)^{6}	3.03(2)	Ba(2)—O(2)^{7}	3.02(2)
Ba(1)—O(4)^{8}	3.03(2)	Ba(2)—O(4)^{12}	3.13(3)
Ba(1)—O(4)^{7}	3.03(2)	Ba(2)—O(4)^{14}	3.13(3)
O(3)^{1}—Ba(1)—O(3)^{2}	115.2(2)	O(5)^{9}—Ba(2)—O(5)^{10}	119.79(8)
O(3)^{1}—Ba(1)—O(5)^{4}	60.5(5)	O(5)^{10}—Ba(2)—O(3)^{12}	61.0(5)
O(3)^{2}—Ba(1)—O(5)^{4}	62.9(5)	O(3)^{12}—Ba(2)—O(3)^{13}	96.0(4)
O(3)^{3}—Ba(1)—O(5)^{4}	115.0(5)	O(5)^{10}—Ba(2)—O(2)^{6}	63.5(6)
O(5)^{4}—Ba(1)—O(5)^{5}	64.2(6)	O(3)^{12}—Ba(2)—O(2)^{6}	59.1(5)
O(3)^{1}—Ba(1)—O(1)^{6}	67.0(5)	O(3)^{14}—Ba(2)—O(2)^{6}	134.6(6)
O(3)^{2}—Ba(1)—O(1)^{6}	116.4(6)	O(2)^{8}—Ba(2)—O(2)^{7}	100.1(5)
O(3)^{3}—Ba(1)—O(1)^{6}	119.0(5)	O(5)^{9}—Ba(2)—O(4)^{12}	57.1(6)
O(5)^{4}—Ba(1)—O(1)^{6}	115.9(5)	O(3)^{13}—Ba(2)—O(4)^{14}	96.4(6)
O(5)—Ba(1)—O(1)^{6}	176.6(6)	O(2)^{7}—Ba(2)—O(4)^{14}	86.9(5)
O(3)^{3}—Ba(1)—O(4)^{6}	172.0(8)	O(4)^{12}—Ba(2)—O(4)^{14}	64.5(8)
O(5)^{4}—Ba(1)—O(4)^{6}	57.9(7)	O(5)^{9}—Ba(2)—O(4)^{13}	98.6(6)
O(1)^{7}—Ba(1)—O(4)^{8}	120.2(9)	O(2)^{7}—Ba(2)—O(4)^{13}	106.2(7)
N(2)—Ni—N(2)^{15}	90.3(6)	N(1)—O(1)—Ba(1)^{17}	118.3(18)
N(2)^{15}—Ni—N(1)	179.3(7)	N(1)—O(1)—Ba(2)^{17}	95(2)
N(1)^{15}—Ni—N(1)^{16}	90.9(7)	N(2)—O(3)—Ba(1)^{18}	124.9(11)
N(2)—Ni—N(1)^{15}	89.0(6)	O(3)—N(2)—Ni	124.9(13)
N(2)^{15}—Ni—N(1)^{15}	89.8(6)	O(1)—N(1)—Ni	121(2)
N(2)^{16}—Ni—N(1)^{15}	179.3(7)	O(2)—N(1)—O(1)	119(2)
N(2)—Ni—N(1)^{16}	179.3(7)	O(2)—N(1)—Ni	119.4(13)
		N(2)—O(4)—Ba(2)^{19}	103(2)

Symmetry code: 1=(1−x, −y, z+1/2); 2=(x−y, x, z+1/2); 3=(y+1,−x+y+1, z+1/2); 4=(−y+1, x−y, z); 5=(−x+y+1,−x+1, z); 6=(y+1, −x+y, z+1/2); 7=(−x, −y, z+1/2); 8=(x−y+1, x+1, z+1/2); 9=(x−y+1, x, z+1/2); 10=(y,−x+y, z+1/2); 11=(−x+1, −y+1, z+1/2); 12=(−x+y+1, −x, z+1); 13=(x+1, y+1, z+1); 14=(−y, x−y, z+1); 15=(−y, x−y, z); 16=(−x+y, −x, z); 17=(−x, −y, z−1/2); 18=(−x+1, −y, z−1/2); 19=(x−1, y−1, z−1); 20=(−x+1, −y+1, z−1/2).

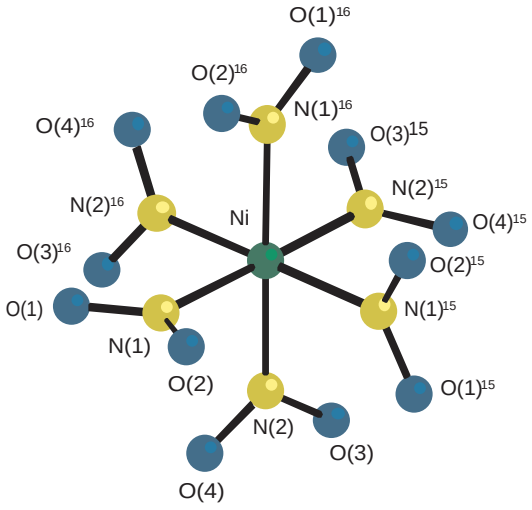

Fig. 2 View of the coordination polyhedron for nickel(II) with atom numbering in $[Ba_2Ni(NO_2)_6(H_2O)_2]\cdot 2H_2O$

1000–1100 cm^{-1}, corresponding to the ν(NO) and at 1400–1500 cm^{-1} to the ν(N=O) vibrations. In the title compounds, the presence of bands only at about 1300 cm^{-1} for all of them is indicative of the metal–ligand coordination through the nitrogen atoms, as was observed in the structural data of the barium compound. The band that appears at 820 cm^{-1} can be attributed to the deformation vibration of the O—N—O group, δ(ONO), in all compounds.

The X-band EPR spectra of the polycrystalline samples show isotropic signals with a variation in the linewidth with decreasing temperature. The spectra of the barium derivative are shown in Fig. 3. No significant variations in the spectra of the other compounds were observed. At room temperatures, nickel(II) compounds usually show broad bands because of the short spin–lattice relaxation times. The obtained g values for the barium compound are 2.166, 2.167 and 2.068, at 293, 100 and 4 K, respectively. A diminution of the linewidth with decreasing temperature is observed until 100 K. Nevertheless, at lower temperatures, an inhomogeneous broadening in the lines can be seen, as was observed in other nickel(II) compounds.[21] This fact might be explained by the different splitting in the ground state of all the paramagnetic centres.

Thermal analysis

The decomposition steps of the title compounds were obtained from the TG curves (Fig. 4) which show the occurrence of two consecutive processes, ligand pyrolysis and inorganic residue formation. For the barium compound the presence of a third step, which corresponds to the loss of the four water molecules, was also observed.

In the anhydrous nitro complexes, the decomposition begins with ligand pyrolysis. This process generally involves different steps which generate a diversity of products, to yield, afterwards, ligand elimination.[22] In these compounds, the breakdown of the nitro complexes generates NiO.[23] Alkali- and alkaline-earth-metal ions remain coordinated to the ligands, which is in good agreement with the theoretical mass losses accompanying the degradation:

$$MM'Ni(NO_2)_6] \rightarrow NiO + M(NO_2)_n + M'(NO_2)_n$$

After this process, an increase in mass is observed in the TG curves obtained under air. This increase may be due to the nitrite–nitrate oxidation reaction, which generally takes place

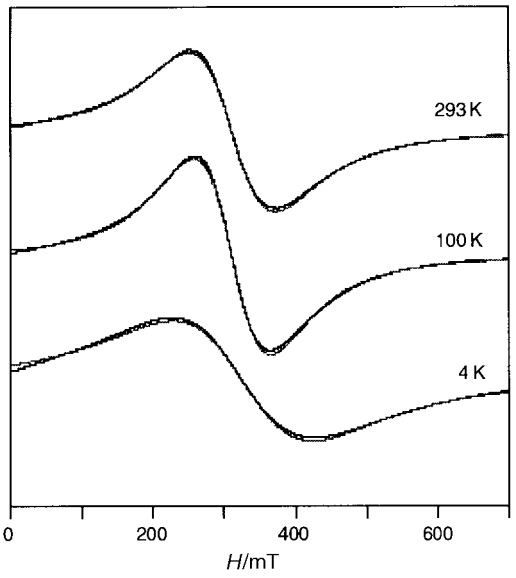

Fig. 3 X-Band spectra of a powdered sample of $[Ba_2Ni(NO_2)_6(H_2O)_2]\cdot 2H_2O$

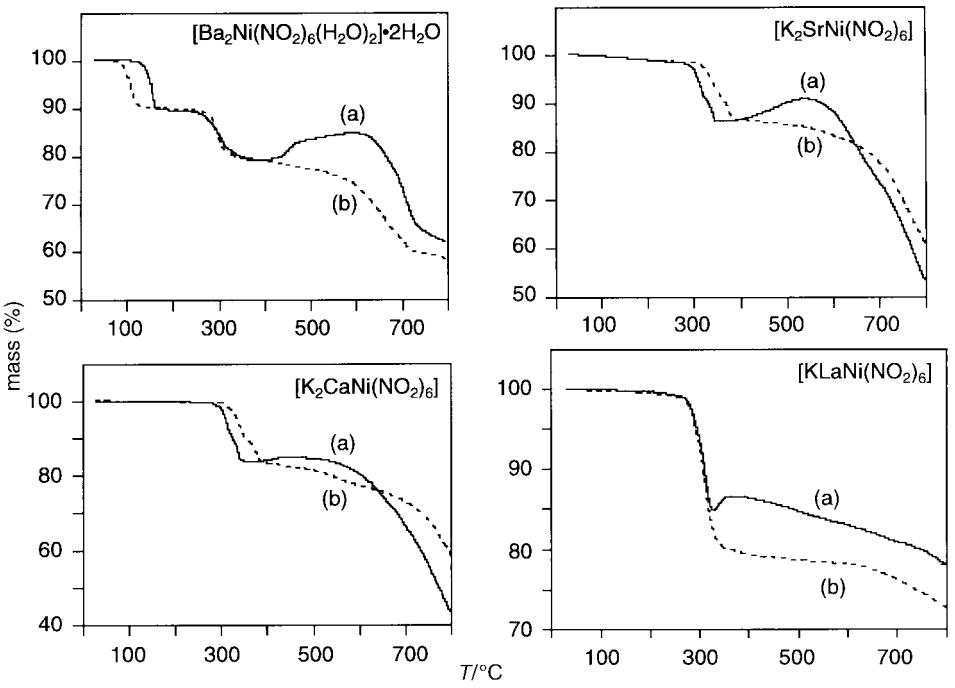

Fig. 4 TG curves of the different compounds (a) in air (—) and (b) in a nitrogen atmosphere (– – –)

between 500 and 600 °C:

$$NiO + M(NO_2)_n + M'(NO_2)_m \rightarrow Ni_{1-x}O + M(NO_3)_n + M'(NO_3)_n$$

This mass increase was not observed in the thermal decomposition performed in nitrogen atmosphere. In the case of the lanthanum compound, the formation of an oxonitrate, $LaO(NO_3)$,[22] could also be possible.

After this step, a continuous mass loss occurs, which can be attributed to nitrate pyrolysis. Understanding of this stage is required for a study of the final products. In this step, no significant differences have been observed in TG analyses performed under different atmospheric conditions. In both cases, the ligand degradation does not seem to be complete, as substantial slopes appear in the TG data. Nevertheless, the characterization of the final products using X-ray diffraction was not possible because of the formation of melts, due to the low melting points of the nitrate compounds.

Evolution of the inorganic residue

In order to obtain pure phases of mixed oxides, the complexes were fired in tubular furnaces at different temperatures. X-Ray diffraction patterns of the products were obtained (Fig. 5) and indexation of the phases was performed in the range $2\theta = 10–70°$.

The thermal decomposition of $[K_2CaNi(NO_2)_6]$ did not lead to the formation of any mixed oxide. After thermal treatment at 500 °C, a mixture of phases formed by KNO_3, $CaCO_3$, CaO and NiO was observed. The calcination of the mixture at 700 and 800 °C led to the disappearance of the nitrate, but modifications in the other phases were not observed. Nevertheless, some peaks of the diffraction patterns could not be indexed with any of the phases cited in the literature.

The thermal treatment of the $[K_2SrNi(NO_2)_6]$ complex at 680 °C yielded a melt formed by KNO_3, $Sr(NO_3)_2$, $SrCO_3$ and NiO. After that, the mixture was calcined at 750 and 800 °C for 2 h at each temperature. The diffraction patterns of the products showed the presence of $Sr_2Ni_2O_5$, $SrCO_3$ and NiO. No peaks corresponding to any potassium phases are present, probably due to the formation of K_2O which sublimes at higher temperatures. Thermal treatment at 900 °C did not yield

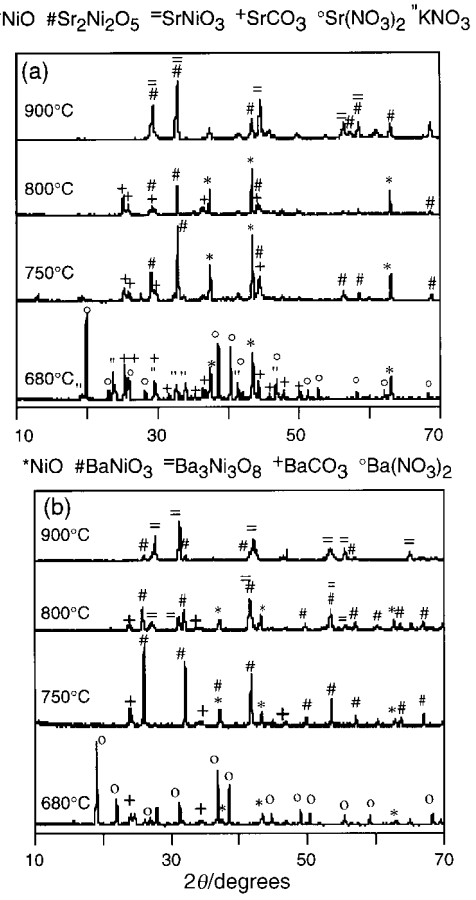

Fig. 5 X-Ray diffraction spectra of the phases obtained at different temperatures from the $[K_2SrNi(NO_2)_6]$ (a) and $[Ba_2Ni(NO_2)_6(H_2O)_2]\cdot 2H_2O$ (b) precursors

the formation of a unique phase of the mixed oxide, but the $Sr_2Ni_2O_5$ phase is a minority phase and the new $SrNiO_3$ oxide is formed. It is important to note that this last compound, which contains tetravalent nickel ions, was only obtained under a high pressure of oxygen (50–2000 atm, 600 °C).[24]

The $[Ba_2Ni(NO_2)_6(H_2O)_2]\cdot 2H_2O$ compound was first heated at 680 °C for 10 h and a melt formed by $Ba(NO_3)_2$, $BaCO_3$ and NiO was obtained. As can be seen, oxidation of the nitrite groups, which was observed in the TG study, and carbonation of a part of the alkaline-earth metal, occur. After, this process the melt was ground and heated at 750 and 800 °C for 2 h. At these temperatures the nitrate decomposes and a mixture of the $BaNiO_3$[25] and $Ba_3Ni_3O_8$[26] oxides, together with the NiO and $BaCO_3$ phases, is obtained. Thermal treatment at 900 °C did not yield a unique phase, with both the $BaNiO_3$ and $Ba_3Ni_3O_8$ oxides obtained. This last oxide is not well defined and seems to be related to the $BaNi_{0.83}O_{2.5}$[6] phase. Taking into account the stoichiometry of these phases ($BaNi_{0.83}O_{2.5}$ and $BaNiO_3$) and that it is not possible to calculate their relative proportions from the diffraction patterns, it is very difficult to establish a relationship between the precursor and the final products, as has been performed in other decompositions.[8,9] In the $BaNi_{0.83}O_{2.5}$ compound the nickel atoms are octahedrally coordinated to the oxygen atoms at distances which could correspond to Ni^{II} and low spin Ni^{III} (observed by EPR measurements) and Ni^{IV}.

Finally, in the case of the $[KLaNi(NO_2)_6]$ compound the $LaNiO_3$ mixed oxide was obtained at 500 °C, together with small amounts of KNO_3 and NiO. At higher temperatures (700 °C) the nitrate decomposes and $LaNiO_3$ becomes the majority phase. The remaining minor peaks correspond to a small amount of NiO phase.

As can be seen, no mixed oxides were obtained from the calcium precursor, as was observed in the literature for CaO–NiO mixtures. This may be due to the small size of the calcium ions. The other compounds led to the formation of mixed oxides with Ni^{III} and Ni^{IV} employing soft conditions of temperature and pressure. According to the literature,[27,28] the attainment of these kinds of compounds by the ceramic method requires higher temperatures and oxygen pressures than those employed in the metallo–organic method. Nevertheless, it, as yet, has not been possible to obtain a unique mixed oxide from the strontium and barium compounds. Further experiments in oxygen atmosphere are being performed in order to improve these results.

Scanning electron microscopy

Scanning electron microscopic photographs of some oxides pellets are shown in Fig. 6. As can be seen, no individual particles were obtained, showing the material in a continuous form only interrupted by cracks. In the case of the Sr–Ni–O system, the sample exhibits compactness. This process could be explained by the progressive sintering of the sample from small particles appearing in the decomposition of the complexes.[29] However, for the La–Ni–O system, powders consisting of small particles with diameter <0.5 μm have been observed. This fact indicates that the sintering process has not started for the latter system.

The morphologic differences observed in these oxides depend on the rate of formation of the final oxide. In the M–Ni–O systems (M = alkaline-earth metal), in which a melt is obtained, the diffusion process is favoured and very reactive small particles are formed. These particles will be easily sintered with increasing temperature. Nevertheless, in the case of lanthanum the combustion of the metallo–organic compound led to a powder in which the diffusion process occurred very slowly.

Concluding Remarks

Compounds containing the nitrite ligand have been synthesized with the aim of obtaining nickel oxides from thermal decomposition. The structure of one of them, $[Ba_2Ni(NO_2)_6(H_2O)_2]\cdot 2H_2O$, has been determined by X-ray diffraction. It consists of a three-dimensional network of metal ions coordinated by nitro ligand bridges. Thermal decomposition of these complexes led to the formation of mixed oxides such as $BaNiO_3$, $SrNiO_3$, $Sr_2Ni_2O_5$ and $LaNiO_3$ at comparatively lower temperatures and oxygen pressures than those observed in the literature from the ceramic method. Scanning electron microscopy has shown the usefulness of soft chemical routes in order to obtain homogeneous and small particles. Some attempts to purify these phases are been carried out by modifiying thermal treatments.

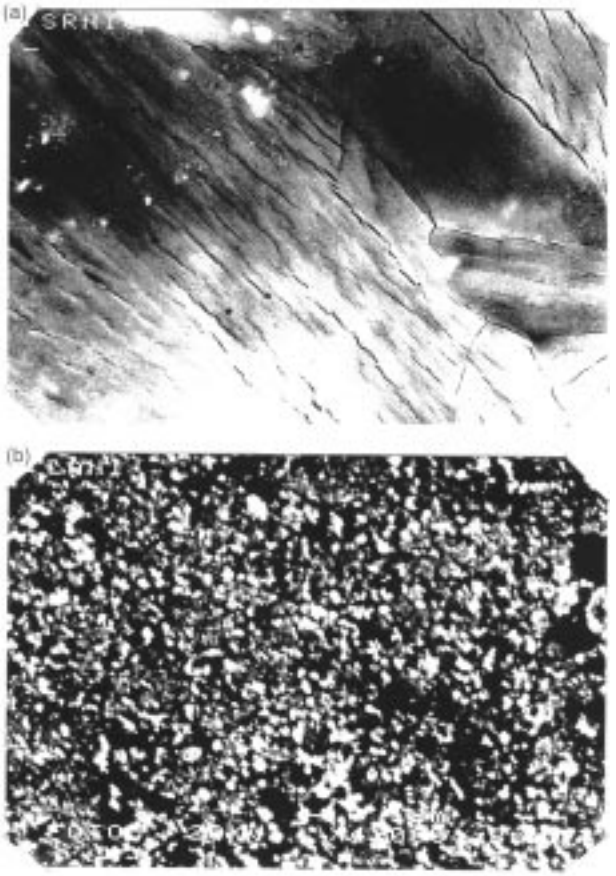

Fig. 6 SEM photographs of the inorganic residue obtained at 800 °C from the precursors: (a) Sr–Ni–O system; (b) La–Ni–O system

This work was financially supported by the DGICYT (PB94–0469) and the Basque Government (PI9640).

References

1 P. Lacorre, J. B. Torrance, J. Pannetier, A. I. Nazzal, P. W. Wang and T. C. Huang, *J. Solid State Chem.*, 1991, **91**, 225.
2 J. B. Torrance, P. Lacorre, A. I. Nazzal, E. J. Ansaldo and Ch. Niedermayer, *Phys. Rev. B*, 1992, **45**, 8209.
3 J. B. Goodenough and P. Raccah, *J. Appl. Phys.*, 1965, **36**, 1031.
4 F. Abraham, S. Minaud and C. Renard, *J. Mater. Chem.*, 1994, **4**, 1763.
5 F. Kananuru, S. Kume and H. Koizumi, *J. Inorg. Nucl. Chem.*, 1972, **34**, 295.
6 J. A. Campá, E. Gutierrez-Puebla, M. A. Monge and I. Rasines and C. Ruiz-Valero, *J. Solid State Chem.*, 1994, **108**, 230.
7 J. García-Jaca, J. I. R. Larramendi, M. Insausti, M. I. Arriortua and T. Rojo, *J. Mater. Chem.*, 1995, **5**, 1995.
8 M. Insausti, J. L. Pizarro, L. Lezama, R. Cortés, E. H. Bocanegra, M. I. Arriortua and T. Rojo, *Chem. Mater.*, 1994, **6**, 707.
9 M. Insausti, R. Cortés, M. I. Arriortua, T. Rojo and E. H. Bocanegra, *Solid State Ionics*, 1993, **63–65**, 351.
10 H. S. Horowitz, S. J. Mclain, A. W. Seeight, J. D. Druliner, L. Gai, M. J. Vankavdaar, J. L. Wagner, R. D. Biggs and S. J. Poon, *Science*, 1989, **243**, 66.
11 S. Takagi, M. Joesten and P. Galen-Lenhert, *Acta Crystallogr., Sect. B*, 1975, **31**, 1970.

12 I. Nakagawa, T. Shinanouchi and K. Yamasaki, *Inorg. Chem*., 1964, **3**, 772; 1968, **7**, 1332.
13 G. M. Sheldrick, *Acta Crystallogr., Sect. A*, 1990, **46**, 467.
14 G. M. Sheldrick, SHELXL96, Program for Refinement of Crystal Structure, University of Göttingen, Germany, 1993.
15 *International Tables for X-ray Crystallography*, Kynoch Press, Birmingham, 1974, vol. IV, pp. 72–98.
16 M. Nardelli, PARST, *Comput. Chem*., 1983, **7**, 95.
17 E. Dowty, ATOMS, A Computer Program for Displaying Atomic Structures, version 2.0, Kingsport, TN, 1993.
18 N. Müller and A. Falk, BALL&STICK, Institute of Chemistry, Johannes Kepler University, Linz, Austria, 1989.
19 E. L. Muetterties and L. J. Guggenberger, *J. Am. Chem. Soc*., 1988, **7**, 1383.
20 J. Rodriguez-Carvajal, FULLPROF, Program Rietveld Pattern Matching Analysis of Powder Patterns, ILL Grenoble, unpublished, 1994.
21 D. Reinen, C. Friebel and K. P. Reetz, *J. Solid State Chem*., 1972, **4**, 103.
22 T. C. Vaimakis, *Thermochim. Acta*, 1992, **206**, 219.
23 H. Langfelderová, *Thermochim. Acta*, 1985, **85**, 75.
24 Powder Diffraction File, card no. 25–904, Joint Committee on Powder Diffraction Standards, Swarthmore, PA, 1984.
25 Powder Diffraction File, card no. 4–817, Joint Committee on Powder Diffraction Standards, Swarthmore, PA, 1984.
26 Powder Diffraction File, card no. 4–684, Joint Committee on Powder Diffraction Standards, Swarthmore, PA, 1984.
27 Y. Takeda, F. Kanamaru, M. Shimada and M. Koizumi, *Acta Crystallogr., Sect. B*, 1976, **32**, 2464.
28 Y. Takeda, T. Hashino, H. Miyamoto, F. Kanamaru, S. Kume and M. Koizumi, *J. Inorg. Nucl. Chem*., 1972, **34**, 1599.
29 F. Thümmler and W. Thomma, *Metallurg. Rev*., 1967, **69**, 115.

Paper 7/02240I; *Received* 2*nd April*, 1997